Magnetic Resonance Imaging of Animal Brain In Vivo

Jens Frahm, Oliver Natt, Takashi Watanabe, Susann Boretius, Thomas Michaelis

Biomedizinische NMR Forschungs GmbH am MPI für biophysikalische Chemie, Göttingen

Since the fundamental discovery of spatial resolution in nuclear magnetic resonance by the 2003 Nobel laureates Paul C. Lauterbur (1) and Peter Mansfield (2) in 1972/73, non-invasive magnetic resonance imaging (MRI) has undergone a tremendous development from a physical tool with potential medical applications to the method of choice and premier modality for diagnostic imaging. Apart from technical advances in instrumentation such as the availability of large-bore superconducting magnets and high-performance gradient coils for spatial discrimination, this development was based on several breakthroughs in MRI physics, in particular the invention of rapid gradient-echo imaging in 1985 (3-5). The underlying principles allowed for a wide range of new applications ranging from breathhold MRI of the thorax and abdomen to EKG-synchronized dynamic imaging of the heart as well as high-resolution three-dimensional (3D) imaging of complex anatomical structures.

Many of the important improvements have first been made in applications to the central nervous system where methods are available that by far extend the possibilities of structural imaging. In fact, such approaches complement the excellent soft-tissue contrast and high pathological sensitivity of conventional MRI by a more specific characterization of brain tissue. For example, aspects of focal brain chemistry may be studied by localized proton MR spectroscopy. Pertinent measurements yield patterns of cerebral metabolites in the millimolar concentration range which are indicative of both the cellular composition and intracellular metabolism. Recently, the axonal connectivities between brain systems became accessible via the diffusion properties of water within white matter. The technique exploits the anisotropic motion of water molecules inside myelinated axons to discriminate white matter from gray matter and to determine the actual fiber direction. And finally, a most significant contribution to cognitive neuroscience stems from the capability to map the functional anatomy of the human brain. The underlying visualization of task- or stimulus-related activations in networks of cortical and subcortical gray matter is based on the use of an

endogenous contrast provided by differences in the concentration of paramagnetic deoxyhemoglobin in the microvasculature.

Why neuroimaging of animals?

Despite the fact that many technical advances in MRI have originally been developed using small-bore magnets suitable for studying laboratory animals, the tremendous success and commercial impact of human MRI has largely masked the fact that - parallel to medical applications – research in neuroimaging of small animals progressed at similar speed. Its key potential and strategic role is to provide a link between system-oriented neurobiology, molecular neurobiology and neurogenetics, and secondly, to close the gap between research on animal models of human disorders and future clinical applications to human patients.
Similar to studies of the human brain, *in vivo* magnetic resonance examinations of anesthetized animals allow for the assessment of anatomic, metabolic, and even functional aspects of the intact central nervous system. The central problems result from the small brain size and correspondingly lower signal-to-noise ratio than obtainable in humans, and the need for anesthesia which in functional studies may hamper the use of the blood flow-mediated approaches commonly in use for humans. For recent applications in rodents see (6).
A main area of research is devoted to neuroimaging of genetically manipulated animals (mice). Complementary to histologic and behavioural studies, MRI is expected to contribute to a better understanding of the morphologic and functional consequences in the intact system. Mutant animal models are designed to allow for a more detailed investigation of the pathophysiology of a particular disorder and a corresponding assessment of novel therapeutic regimens. In this context, the specific potential of MRI is based on its noninvasiveness which offers not only *in vivo* findings but also intraindividual follow-up evaluations which often are more relevant for human applications than mere group analyses. Moreover, the similarity of MRI techniques and image properties for animal and human brain ensures an almost immediate transfer of experimental methods and findings to whole-body MRI systems and patient studies. The following sections briefly discuss selected examples from our laboratory including primates, mice, and insects.

Methodological considerations

MRI requires the positioning of the animal into a strong magnetic field in order to polarize the nuclear spins of water protons. Short radiofrequency pulses are

then used to disturb the resulting equilibrium magnetization. The subsequent return to equilibrium is termed relaxation and associated with the emission of a radiofrequency signal from the sample itself.

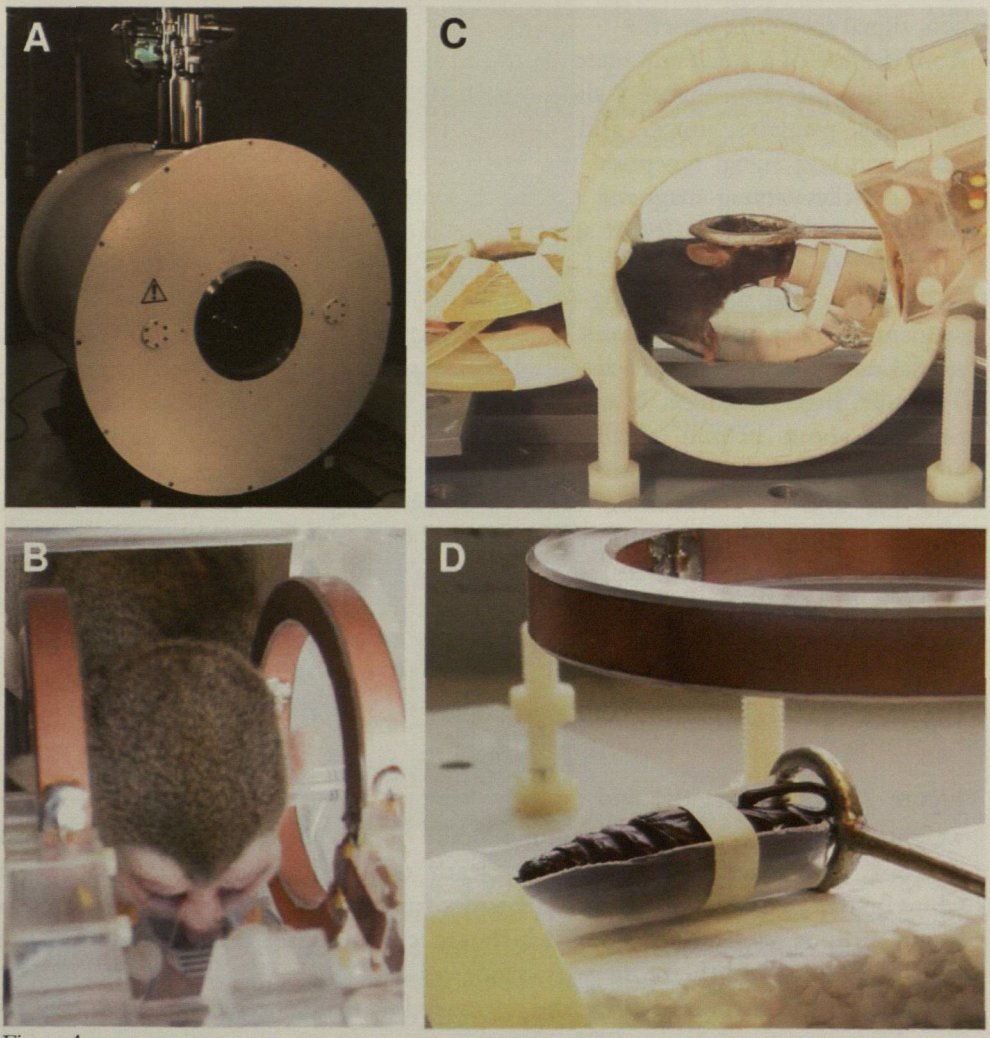

Figure 1.
(A) Small bore (40 cm diameter) magnet for *in vivo* MRI of laboratory animals. The maximum accessible bore has a diameter of 20 cm because of the magnetic gradient coils required for spatial assignment. (B-D) Experimental setup (B) for small primates using a single homogeneous Helmholtz coil (10 cm diameter) for radiofrequency excitation and signal reception, (C) for mice using a Helmholtz coil (10 cm diameter) for excitation and an elliptical surface coil (12 mm short axis, 20 mm long axis) for reception, and (D) for insects using a similar arrangement with a circular surface coil (16 mm diameter) oriented perpendicular to the long axis of the animal.

While primates and rodents are studied under general anesthesia, narcosis is not required for *Manduca sexta* in the pupal state.
Excitation and detection are accomplished by antennae circumscribing the head of the animal. While homogeneous signal excitation is performed with a large coil, signal reception benefits
from the use of a small coil matched to the size of the brain to obtain an optimal signal-to-noise ratio. Figure 1 shows the coil arrangements for MRI of the brain of small primates, mice, and insects, respectively. During radiofrequency excitation and signal reception the MRI experiment employs three orthogonal and spatially varying magnetic fields for a spatial discrimination of the signal. Multiple signals with different spatial encodings need to be recorded for image reconstruction.
It turns out that neuroimaging of small animals clearly benefits from 3D MRI sequences. They provide access to a sufficiently high (and preferably isotropic) spatial resolution in order to resolve the major cerebral structures of interest (7). Typically, high-resolution *in vivo* studies with adequate signal require measuring times of about 30 min (small primates) to 3 hours (insects). It is possible to achieve a similar range of contrasts as in humans including image weightings with T1, T2, and T2* relaxation times as well as spin density (that is water concentration), magnetization transfer with information about the macromolecular content (8), and diffusion indicating differences in water mobility (9-11). Functional studies rely on changes in deoxyhemoglobin (6) or the application of exogenous contrast agents (12-16).

Primate brain: diffusion tensor mapping of axonal connectivities

Figure 2 shows a sagittal and (slightly magnified) coronal section from a T1-weighted 3D MRI acquisition of the brain of a squirrel monkey at 234 µm isotropic resolution. The anatomy is clearly depicted with high intensities for white matter structures and lower intensities for gray matter. Bright spots refer to water protons in flowing blood which are continuously refreshed during the imaging process and therefore mark major vessels.
The good signal-to-noise ratio at the relatively low magnetic field strength of 2.35 T is due to the much longer T2* relaxation time of brain tissue than observed at higher fields. Thus, the use of optimized MRI sequences with small receiver bandwidths and correspondingly reduced noise level effectively counterbalances the (linear) decrease of the equilibrium magnetization at lower fields. Moreover, lower magnetic fields exhibit a reduced sensitivity to magnetic field

inhomogeneities and associated susceptibility artefacts. Such problems occur at air-tissue boundaries and may severely degrade the quality of high-field gradient-echo images of animal brain.

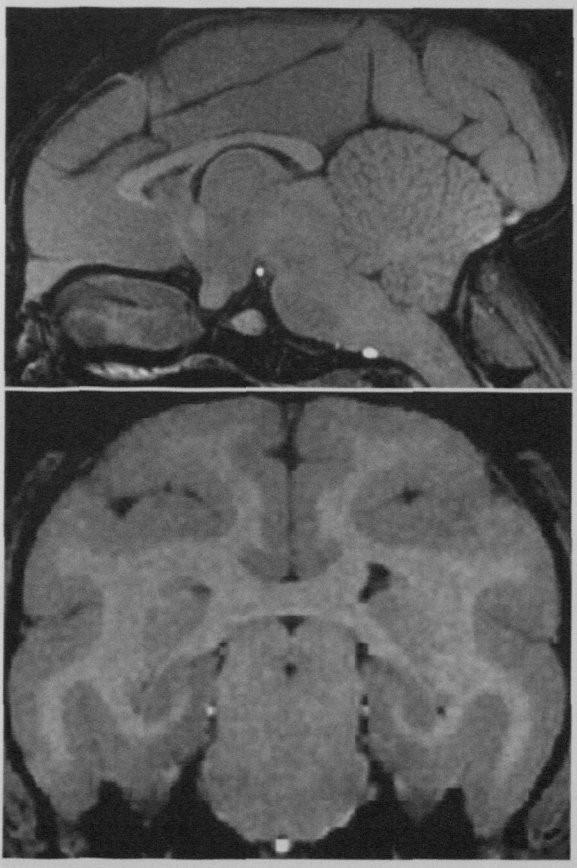

Figure 2. T1-weighted 3D MRI (FLASH, TR/TE = 23/10.1 ms, 25° flip angle) of the brain of a squirrel monkey *in vivo* at 234 μm isotropic resolution in (top) a sagittal and (bottom) a coronal section orientation. Although the central nervous system exhibits a much less pronounced gyrification than a human brain, it closely resembles its structural organization. In particular, the coronal section reveals good contrast between cortical gray matter (gray intensity) and white matter (bright intensity).

Diffusion-weighted MRI allows for a more detailed look into the structural organization of white matter in animal brain *in vivo* (9-11). Diffusion measures the microscopic motion of water (protons) within brain tissue. Rather than simply determining the mean speed or motion-induced positional displacement for a given diffusion time, diffusion MRI studies that employ multiple gradient directions offer the advantage of mapping the diffusion tensor, that is a set of orientation-dependent diffusion coefficients along 6 principal axes. This quantity may be used to identify regions of anisotropic water mobility which in brain tissue mainly applies to white matter where bundles of elongated and heavily myelinated axons facilitate the motion of water molecules along the long axis of the axon but not perpendicular to it.

In comparison with T1-weighted anatomical images of the brain of a squirrel monkey (top), Figure 3 confirms that motional anisotropy in diffusion anisotropy maps (middle) predominantly refers to white matter. In the selected sections the highest degree of anisotropy
(coded in bright intensities) is seen in the anterior commissure connecting both hemispheres. Gray matter exhibits no pronounced motional anisotropy, at least not over the spatial dimension of an MRI voxel.

Figure 3.
(Top) MRI anatomy (T1), (middle) relative anisotropy (RA) of the water diffusion highlighting white matter, and (bottom) color-coded mean diffusion direction (MDD) of nerve fibers in two coronal brain sections of a squirrel monkey *in vivo* (11.5 mm and 4.5 mm anterior to the external auditorial meatus). CC = corpus callosum, Ci = internal capsule, CA = anterior commissure, CH = optical chiasm, PC = cerebral peduncle, CSP = corticospinal tract, BP = brachium pontis, SSP = stratum superficiale pontis.

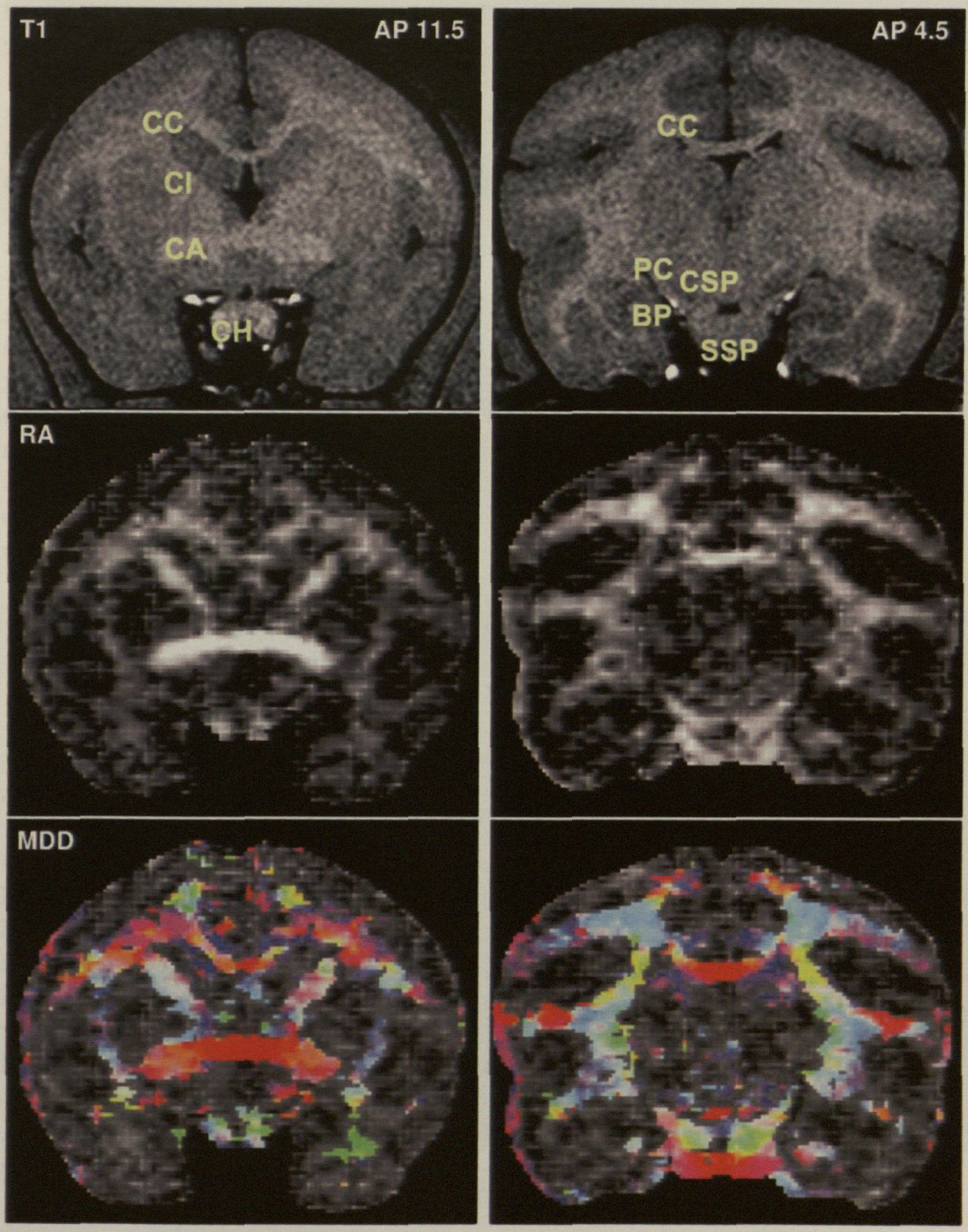
T1
AP 11.5
CC
CI
CA
CH
AP 4.5
CC
PC
CSP
BP
SSP
RA
MDD

It should also be noted that the scalar value of the diffusion coefficient is very similar in gray and white matter. Marked differences are only seen in pathological situations such as ischemia which renders diffusion MRI an indispensible tool for the early detection of ischemic lesions in acute stroke.
Because the diffusion tensor contains information about the orientation dependence of the molecular motion, it is possible to calculate not only a qualitative anisotropy map (where do we have anisotropic motion?) but also a quantitative map of the main diffusion orientation (in which direction are water molecules preferentially moving?). Using a color code, this information is visualized in the bottom part of Fig. 3. For example, coding the right-to-left (or left-to-right) direction in red identifies the interhemispheric connections in the corpus callosum and anterior commissure. Under the assumption that these main diffusion directions coincide with the long axis of white matter fiber tracts, it becomes possible to iteratively `trace' axonal connections from a starting point in a selected voxel (or region) via suitable neighborhood algorithms. Although pertinent approaches are technically feasible and already led to fascinating maps of the structural connectivity in human brain, they are still very demanding and so far only few attempts have been made to unravel connectivities in animal brain *in vivo*.

Mouse brain: functional mapping of neural projections

When studying murine brain, the key problem is spatial resolution (7,8). Together with a surface coil for signal reception which matches the desired field-of-view, 3D MRI acquisitions with measuring times of 1-1.5 hours provide a sufficiently high signal-to-noise ratio for an isotropic resolution of 100-150 μm. Figure 4 compares corresponding acquisitions for two different mouse strains in selected sagittal, horizontal, and coronal sections. The data unravel pronounced neuroanatomical variations which here refer to much larger ventricular spaces in C57BL/6J mice than in BALB/c mice. In general, many important cerebral microstructures are well delineated including the external capsule, anterior commissure, corpus callosum, hippocampal fimbria, hippocampal formation, and cerebellar sulci (7). Although the results support a slight tendency in favor of T1-weighted gradient-echo MRI sequences for a delineation of the neuroanatomy, the usefulness and sensitivity of T2-weighted spin-echo sequences for the detection of pathologic alterations is well appreciated.

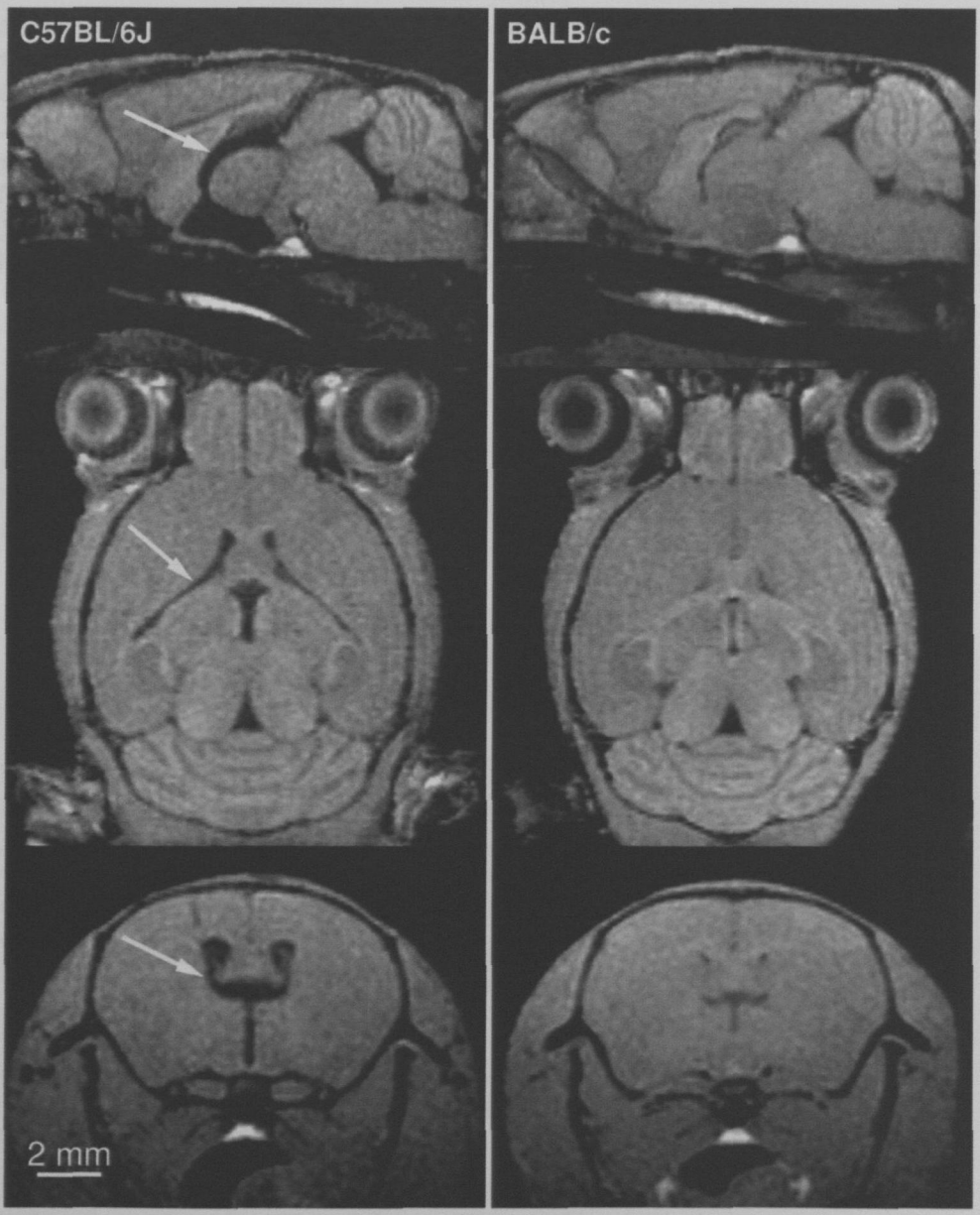

Figure 4. T1-weighted 3D MRI (FLASH, TR/TE = 17/7.6 ms, 25° flip angle) of the brain of (left) a C57BL/6J and (right) a BALB/c mouse *in vivo* at 117 µm isotropic resolution. The comparison demonstrates structural variations in different strains such as larger ventricular spaces in the forebrain of C57BL/6J mice (arrows). The images refer to (top) a mid-sagittal position, (middle) a horizontal section, and (bottom) a coronal section.

In contrast to human studies, functional mapping of mouse brain may be accomplished by using exogenous (paramagnetic) contrast agents such as divalent mangenese ions (12-14). These T1-shortening MRI contrast media are known to be taken up by excitable cells (neurons) via voltage-gated calcium channels. Moreover, depending on brain function, manganese ions are transported along axonal projection pathways which therefore become highlighted in T1-weighted images. Because of the limited speed of axonal transport mechanisms, manganese-enhanced MRI is usually performed several hours after the original manganese administration.

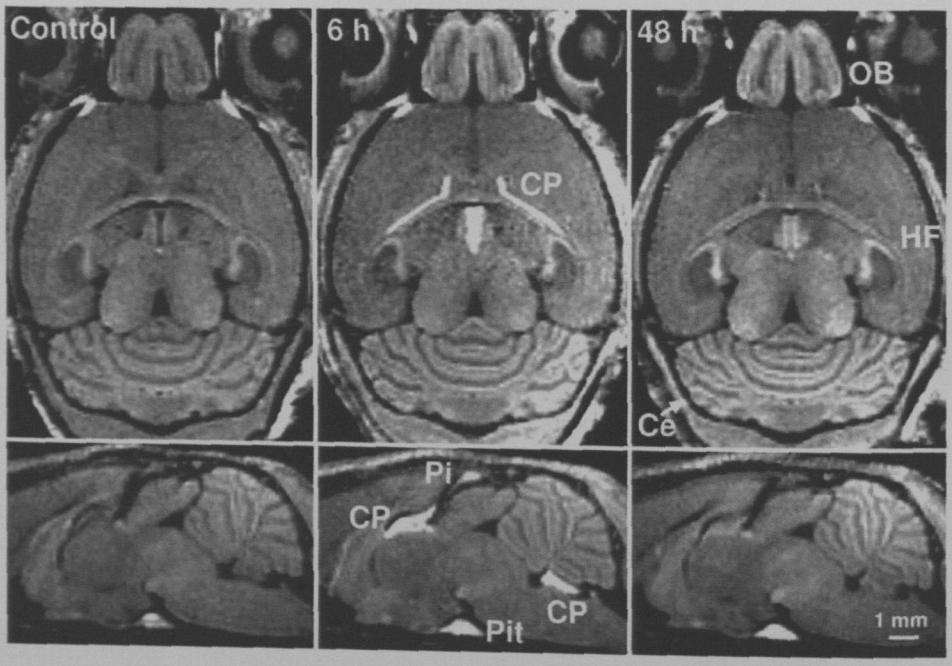

Figure 5.
Manganese-induced MRI signal enhancement of the brain of an NMRI mouse (left) before as well as (middle) 6 hours and (right) 48 hours after subcutaneous injection of 5 ml/kg body weight $MnCl_2$ (20 mM) in (top) horizontal and (bottom) midsagittal sections (T1-weighted 3D FLASH, TR/TE = 22/8.2 ms, 30° flip angle, 120 µm isotropic resolution). In contrast to the transient MRI signal enhancement in the choroid plexus (CP), pineal gland (Pi), and anterior pituitary gland (Pit), brain tissues with a blood-brain barrier such as the olfactory bulb (OB), dentate gyrus and CA3 subregion of the hippocampal formation (HF), and cerebellum (Ce) exhibit a delayed and more persistent enhancement.

Figure 5 reveals both short-term and long-term MRI signal enhancements in mouse brain before as well as 6 hours and 48 hours after systemic (subcutaneous) application of a single dose of $MnCl_2$ (15). At 6 hours after administration (center column), tissues without a blood-brain barrier such as the choroid plexus, pineal gland, and anterior pituitary gland show a pronounced enhancement. On the other hand, brain regions such as the olfactory bulb, hippocampal formation, and cerebellar cortex reveal an enhancement only in later examinations (right column). For example, at 48 hours, the manganese enhancement improves the delineation of the layered structures within the cerebellum as the outer bright layer circumscribes an interior region without a substantial signal increase. Most likely, the bright signal represents the uptake and accumulation of mangenese ions within the cerebellar cortex, while the interior non-enhancing areas refer to white matter. Further insights into the functional connectivity of mouse brain may be gained by direct intracerebral injections into the posterior hippocampus which have been shown to identify the hippocampal projection pathways into the lateral septum (16).

Insect brain: towards mapping neurodevelopment

In comparison with mammals, the insect brain reveals a much simpler organization. With seeing and smelling as key functions which require central processing of sensory information, the optical and antennal lobe form the primary integration centers for the visual and olfactory system, respectively. In this context, *Manduca sexta* serves as a model for the development of the olfactory system which is formed during a 21-day period of metamorphosis. This phase marks the transition from the larva to the adult sphinx moth and is usually divided into pupal stages P0 to P20.

Figure 6 shows selected sections from a 3D MRI acquisition at 100 µm isotropic resolution (1 nl voxel volume) of the brain of a live *Manduca sexta* at pupal stage P12 (17). Apart from highlighting the developing retina, the optical and antennal lobes as well as the antennal nerves are readily discernible in both hemispheres. In fact, after completion of synaptogenesis at about pupal stage P12, even substructures of the central brain such as the calyces of the mushroom bodies (Ca) which possess a similarly high synaptic density as the antennal lobes are well depicted.

Although these findings support the potential of high-resolution 3D MRI to allow for an *in vivo* morphologic characterization of the brain of insects, its use in entomology is not intended to compete with conventional microscopic techniques but to provide new complementary information. For example,

together with the use of T1 contrast agents such as manganese, the MRI protocols are expected to help unravelling the developing neuroaxonal connectivity and brain function during metamorphosis. Current projects focus on functional studies of the evolving olfactory system of *Manduca sexta* after specific labelling of olfactory receptor neurons.

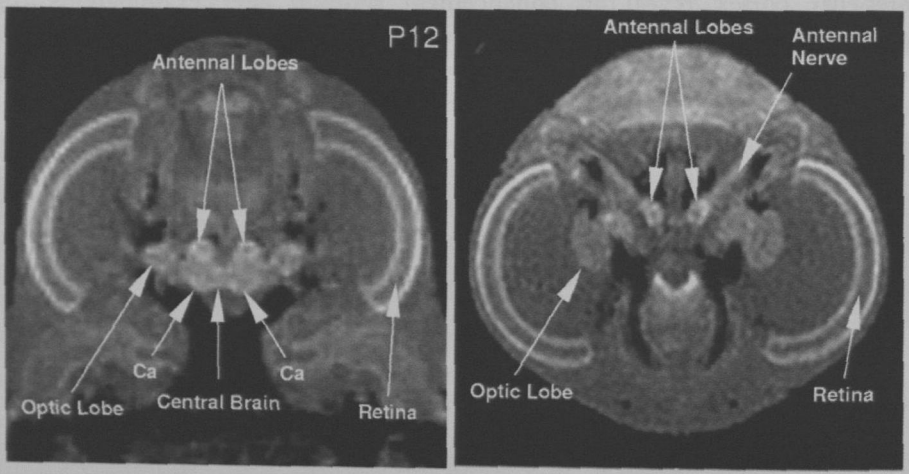

Figure 6.
(Left) Coronal and (right) transverse section of a T1-weighted 3D MRI data set of *Manduca sexta* during metamorphosis at pupal stage P12 (FLASH, TR/TE = 20/7.8 ms, 25° flip angle, 100 µm isotropic resolution). Apart from visualizing major structures such as the developing retina, 3D MRI allows for the identification of the antennal nerves, antennal lobes, optic lobes, and central brain (Ca = calyces of the mushroom bodies).

Acknowledgements

The authors would like to thank Dr. Roland Tanner for his support in performing MRI studies of squirrel monkeys and Dr. Joachim Schachtner for his manifold contributions to MRI studies of insect brain.

References

1. Lauterbur PC. Image formation by induced local interactions: Examples employing nuclear magnetic resonance. Nature 242: 190-191, 1973.
2. Mansfield P, Grannell PK. `Diffraction' and microscopy in solids and liquids by NMR. Phys. Rev. 12: 3618-3634, 1975.
3. Frahm J, Haase A, Hänicke W, Merboldt KD, Matthaei D. Hochfrequenz-Impuls und Gradienten-Impuls-Verfahren zur Aufnahme von schnellen NMR-Tomogrammen unter Benutzung von Gradientenechos. German Patent Application P 3504734.8, February 12, 1985.
4. Frahm J. Rapid FLASH NMR imaging. Naturwissenschaften 74: 415-422, 1987.
5. Frahm J. Toward rapid NMR imaging. NMR Encyclopedia 1: 318-322, 1996.
6. Ahrens ET, Narasimhan PT, Nakada T, Jacobs RE. Small animal neuroimaging using magnetic resonance microscopy. Progr. NMR Spectr. 40: 275-306, 2002.
7. Natt O, Watanabe T, Boretius S, Radulovic J, Frahm J, Michaelis T. High-resolution 3D MRI of mouse brain reveals small cerebral structures in vivo. J. Neurosci. Meth. 120: 203-209, 2002.
8. Natt O, Watanabe T, Boretius S, Frahm J, Michaelis T. Magnetization transfer MRI of mouse brain reveals areas of high neural density. Magn. Reson. Imaging 21:1113-1120, 2003.
9. Nolte UG, Finsterbusch J, Frahm J. Rapid isotropic diffusion mapping without susceptibility artifacts. Whole brain studies using diffusion-weighted single-shot STEAM MR imaging. Magn. Reson. Med. 44: 731-736, 2000.
10. Boretius S, Watanabe T, Natt O, Michaelis T, Finsterbusch J, Frahm J. Diffusion tensor mapping of living mouse brain using half-Fourier single-shot STEAM MRI. Proc. Intl. Soc. Magn. Reson. Med. 10:1231, 2002.

11. Boretius S, Natt O, Watanabe T, Frahm J, Tammer R, Ehrenreich L, Michaelis T. Diffusion tensor MR imaging: Preliminary applications to mice, rats, and squirrel monkeys. Proc. Göttingen Neurobiol. Conf. 29: 682, 2003.
12. Lin YJ, Koretsky AP. Manganese ion enhances T1-weighted MRI during brain activation: an approach to direct imaging of brain function. Magn. Reson. Med. 38: 378-388, 1997.
13. Pautler RG, Silva AC, Koretsky AP. *In vivo* neuronal tract tracing using manganese-enhanced magnetic resonance imaging. Magn. Reson. Med. 40: 740-748, 1998.
14. Watanabe T, Michaelis T, Frahm J. Mapping of retinal projections in the living rat using high-resolution 3D gradient-echo MRI with Mn^{2+}-induced contrast. Magn. Reson. Med. 46: 424-429, 2001.
15. Watanabe T, Natt O, Boretius S, Frahm J, Michaelis T. *In vivo* 3D MRI staining of mouse brain after subcutaneous application of $MnCl_2$. Magn. Reson. Med. 48: 852-859, 2002.
16. Watanabe T, Natt O, Radulovic J, Spiess J, Boretius S, Michaelis T, Frahm J. 3D MRI of murine hippocampal subfields and projections *in vivo* using Mn^{2+} contrast. Proc. Intl. Soc. Magn. Reson. Med. 10: 1254, 2002.
17. Michaelis T, Watanabe T, Natt O, Boretius S, Frahm J, Utz S, Schachtner J. Brain development during metamorphosis: A 3D MRI study of *Manduca Sexta* at 1 nl resolution. Proc. Intl. Soc. Magn. Reson. Med. 11: 500, 2003.